doi:10.55385/kastamonujes.1123018 KUJES 8(2):90-97, 2022

Kastamonu University
Journal of Engineering and Sciences
e-ISSN 2667-8209
http://dergipark.gov.tr/kastamonujes

Synthesis of Cu-Cr-B_4C-CNF hybrid composites

Osama Ali Ehbil Kriewah[a], Serkan Islak[b,*]

[a] Department of Materials Science and Engineering, Institute of Science, Kastamonu University, Kastamonu, Türkiye
[b] Department of Mechanical Engineering, Faculty of Engineering and Architecture, Kastamonu University, Kastamonu, Türkiye

***Corresponding Author:** serkan@kastamonu.edu.tr

Received: **May 30**, 2022 ◆ Accepted: **September 26**, 2022 ◆ Published Online: **December 26**, 2022

Abstract: In this study, the microstructural properties of Cu-Cr-B_4C-CNF hybrid composites produced by powder metallurgy were investigated. While microstructural properties were examined by optical, SEM-EDS and XRD analyzes, hardness test was performed to determine the mechanical properties. The microstructure results, especially the EDS-MAP analysis, showed that the reinforcement elements were relatively homogeneously dispersed in the copper matrix. Since carbon nanofiber has nano size, it was detected in SEM photographs with larger magnification. Cu, CrB_2, Cr_2B_3 and C phases were detected in the microstructure. The hardness of the composite increased with the addition of reinforcement and reached a maximum value (72.5 HB) of 1% of CNF, and after this CNF ratio, a very small decrease in the hardness value occurred. Compared to the undoped copper sample, the hardness value of the Cu-8B_4C-6Cr-1CNF hybrid composite increased by approximately 54%.

Keywords: Hybrid composite, Copper, CNF, B_4C, Synthesis.

Öz: Bu çalışmada toz metalürjisi ile üretilen Cu-Cr-B_4C-CNF hibrit kompozitlerin mikroyapı özellikleri araştırılmıştır. Mikroyapı özellikleri optik, SEM-EDS ve XRD analizleri ile incelenirken, mekanik özelliklerin tespiti için sertlik testi yapılmıştır. Mikroyapı sonuçları, özellikle EDS-MAP analizi takviye elemanlarının bakır matrisi içerisinde nispeten homojen dağıldığını göstermiştir. Karbon nanofiber nano boyuta sahip olduğu için daha büyük büyütmeli SEM fotoğraflarında tespit edilmiştir. Mikroyapıda Cu, CrB_2, Cr_2B_3 ve C fazları tespit edilmiştir. Kompozitin sertlikleri takviye ilavesiyle artış göstermiş ve CNF'nin % 1 oranında maksimum değere (72.5 HB) ulaşmış, bu CNF oranından sonra sertlik değerinde çok az miktarda azalma meydana gelmiştir. Katkısız bakır numuneye göre Cu-8B_4C-6Cr-1CNF hibrit kompozitin sertlik değerinde yaklaşık %54 artış meydana gelmiştir.

Anahtar Kelimeler: Hibrit kompozit, Bakır, CNF, B_4C, Sentez

1. Introduction

Pure copper is widely utilized in various electrical applications due to its high electrical and thermal conductivities [1]. Copper also has a range of other useful properties, such as high corrosion resistance, low cost, and ease of manufacture. Owing to its distinctive properties, copper is described as a significant engineering material and will continue to be relevant to future technological advances [2,3]. Copper and its alloys are widely used for various applications, such as automobile radiators, heat exchangers, home heating systems, and solar panels [4].

Even though copper has many excellent properties, its ductility makes it vulnerable to mechanical stresses [5]. Therefore, there are a great number of studies on copper alloys and copper matrix composite materials. Precipitation hardening improves the strength of copper alloys by adding different alloying elements into copper. Azimi and Akbari [6] used a mechanical alloying method to produce Cu-Zr alloys for use in the welding industry. While samples mechanically alloyed for 48 hours reached their maximum hardness, hardness declined after that period. Islamgaliev et al. [7] examined the effect of nanostructure formation by high-pressure torsion on strength and electrical conductivity in Cu-Cr alloy. Dynamic precipitation was observed to improve strength and electrical conductivity. However, these precipitates decompose in high-temperature applications, resulting in a decline in strength [8]. Copper matrix composite materials have gained significance in order to overcome this problem. Reinforcements such as carbide [9], oxide [10], nitride [11], carbon nanotubes [12], graphene [13], and diamond [14] have been added into copper in the literature. On a macro-scale, metal matrix composite materials are made up of a metal or alloy matrix and mostly particulate reinforcement material; on a micro-scale, hybrid composites are made up of more than one reinforcing element with distinct properties added to the matrix [15].

In this study, a powder metallurgy (PM) method was used to produce hybrid composites by adding Cr, B_4C, and CNF into copper. The microstructure properties of the hybrid composites so produced were then thoroughly examined.

2. Material and Method

Material

In this study, Cu was used as the matrix (-325 mesh grain size and 99.99% purity) and B_4C (-325 mesh grain size and 99.99% purity), Cr (-325 mesh grain size and 99.99% purity), and CNF (DxL 100 nm×20–200 μm size, 98% purity) were used as reinforcements. Cu, Cr, and B_4C powders were obtained from Nanography and CNF from Sigma-Aldrich. Figure 1 shows scanning electron microscopy (SEM) images of the powders used in the present study. The Cu powder had a wormlike morphology, while Cr and B_4C were sharp edged and CNF was fibrous. Different rates of Cr, B_4C, and CNF were added to Cu. Table 1 shows the powder mixture ratios.

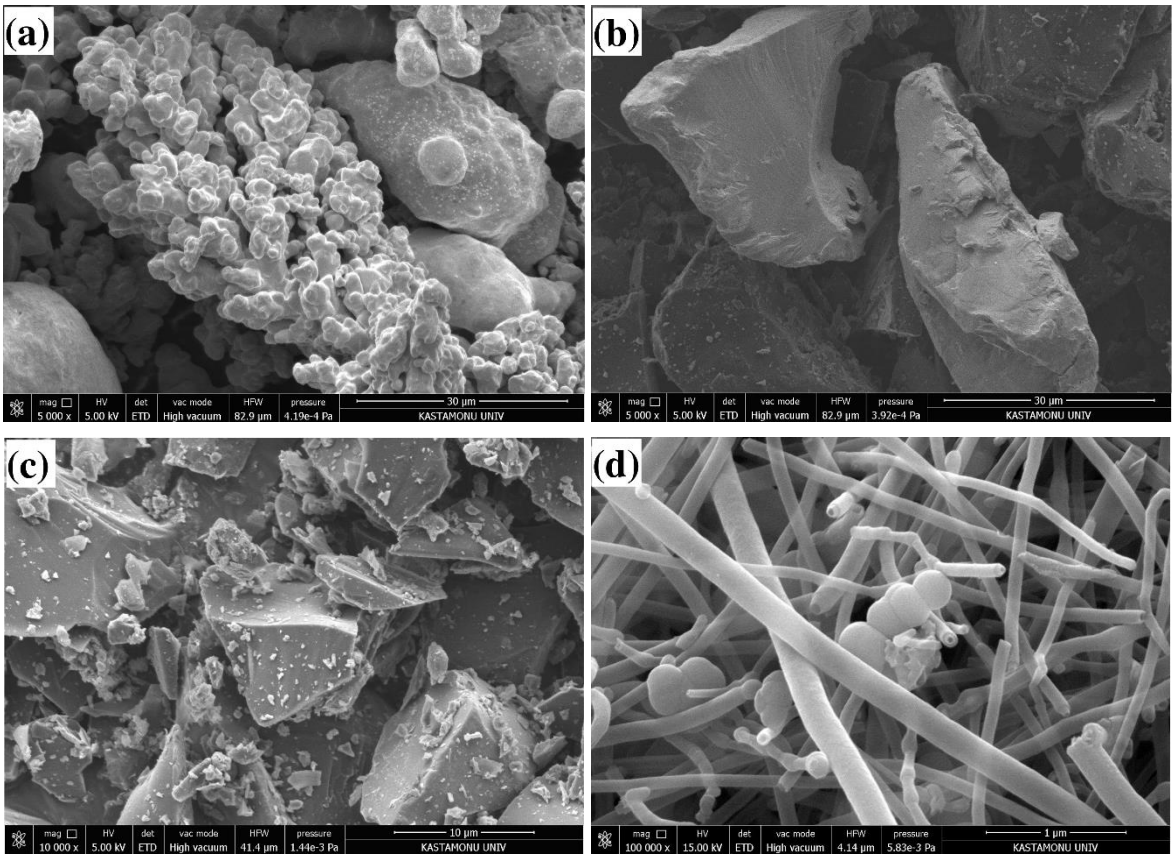

Figure 1. SEM images of the powders: (a) Cu, (b) Cr, (c) B_4C, and (d) CNF

Table 1. Powder mixture ratios (% by volume)

No	Cu	B_4C	Cr	CNF
1	100	0	0	0
2	92	8	0	0
3	90	8	2	0
4	88	8	4	0
5	86	8	6	0
6	85	8	6	1
7	84	8	6	2
8	83	8	6	3

The powders were mixed at the appropriate mixture ratios for 2 hours at 400 rpm using a Retsch PM 100 model mechanical alloying device. 10mm diameter 100Cr6 balls were utilized in the mixture process, with the powder-ball ratio set at 1:5. In order to prevent cold welding and burning of the powders, 2% zinc stearate was added to the powder mixtures before mixing. Mechanically alloyed powder mixtures were pressed in a Specac GS15011 model hydraulic press under 400 MPa pressure, producing samples with a diameter of 20 mm and a height of 10 mm. The green pellet samples were sintered in a Protherm high-temperature tube furnace at 900 ºC for two hours at a heating/cooling rate of 10 ºC/min under an argon atmosphere.

For microstructure analysis, the samples were sanded using 320-2400 mesh sandpaper and polished using a 1-micron diamond solution. The polished samples were etched in a solution containing 100 mL distilled water + 25 mL hydrochloric

acid + 8 g iron (III) chloride. X-ray diffraction (XRD) analysis was performed using the Rigaku Ultra IV XRD. The Carl Zeiss Ultra PLus Gemini FE-SEM was used for SEM and energy dispersive spectrometry (EDS) analyses. Optical microscope examinations of the samples were performed using a Nikon brand inverted metallurgical microscope. Sintered densities were measured using an AND GR-200 balance with a density measuring kit at 10^{-4} precision in accordance with the Archimedes' principle established in the ASTM B 962-17 standard [16]. The hardness of the samples was measured with a Qness Q250 M hardness device under 62.5 kgf load and using 2.5 mm balls as Brinell according to TS EN ISO 6506-1 standard [17]. The work flow chart of the experimental work stages is shown in Figure 2.

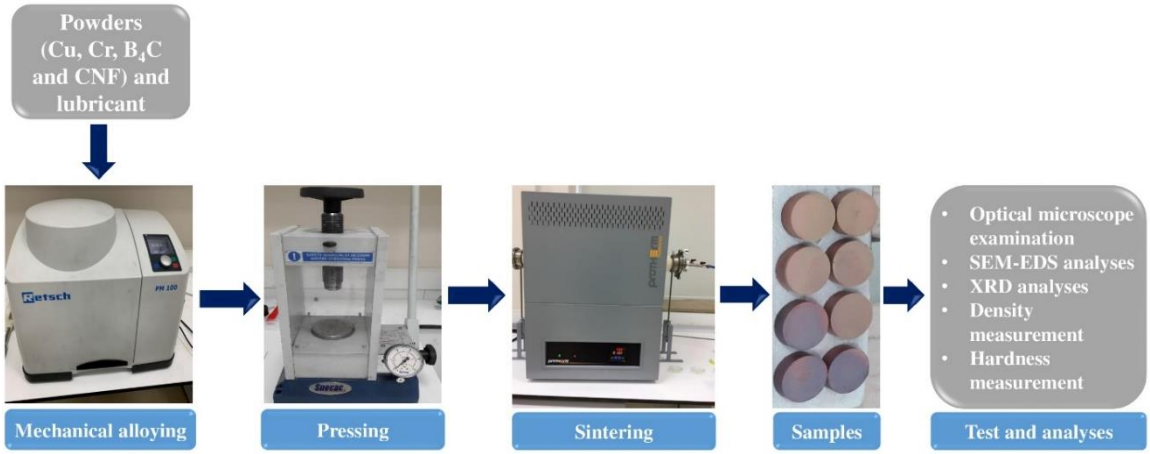

Figure 2. Work flow chart of experimental work stages

3. Result and Discussion

Figure 3 shows optical images of hybrid composites with different reinforcing types and quantities produced by PM. The matrix and reinforcing elements were located in microstructures of different colours. The Cu matrix was reddish, B_4C was dark grey, and Cr was light grey. The optical images show that the B_4C grains were homogeneously dispersed in the Cu matrix; Cr, on the other hand, was relatively homogeneously dispersed, and with increased Cr rates, it was observed to be dispersed in the form of agglomerations in some parts of the samples. SEM examination was performed at high magnification for Sample 6 in order to detect CNFs. Figure 4 shows SEM images of Sample 6. Although CNFs were originally longer, mechanical alloying caused them to be embedded in the copper matrix in a shortened form.

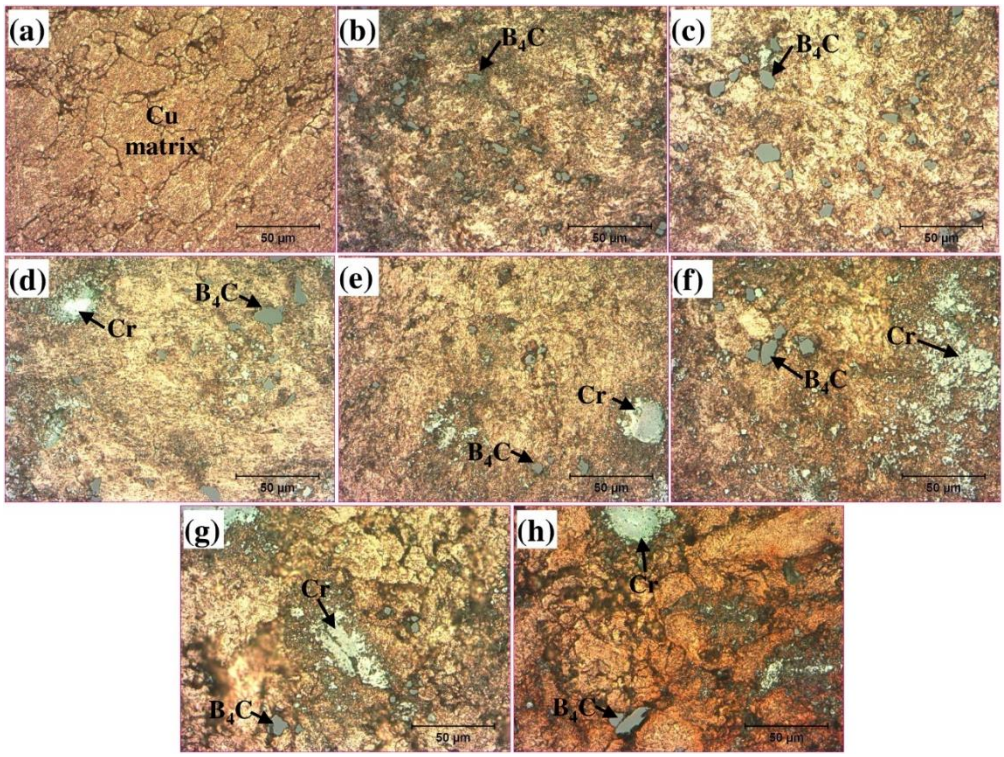

Figure 3. Optical images: (a) Pure Cu, (b) Cu-8B_4C, (c) Cu-8B_4C-2Cr, (d) Cu-8B_4C-4Cr, (e) Cu-8B_4C-6Cr, (f) Cu-8B_4C-6Cr-1CNF, (g) Cu-8B_4C-6Cr-2CNF, and (f) Cu-8B_4C-6Cr-3CNF

Figure 5 depicts a MAP-EDS analysis of the samples to provide information on the distribution of reinforcements in the Cu matrix. The pattern of distribution here broadly corresponds to the optical images. The mechanical and physical properties of the sample are improved by the homogenous distribution of the reinforcing elements in the matrix [18,19]. No crack formation was observed in the microstructure. However, pores formed in all samples.

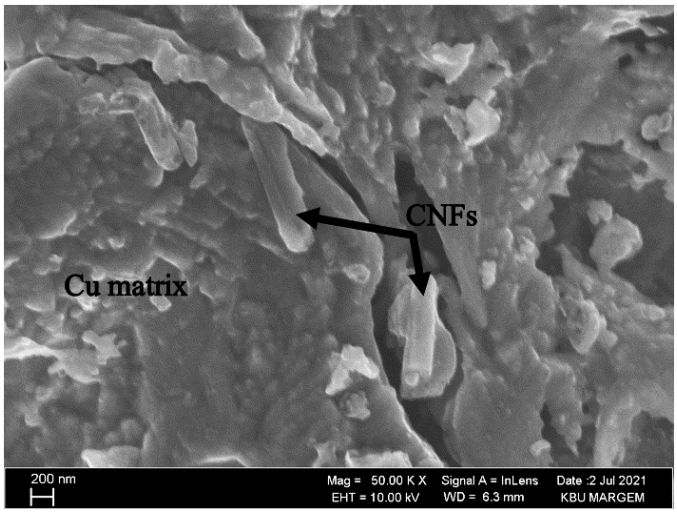

Figure 4. SEM images of Sample 6 (Cu-8B_4C-6Cr-1CNF)

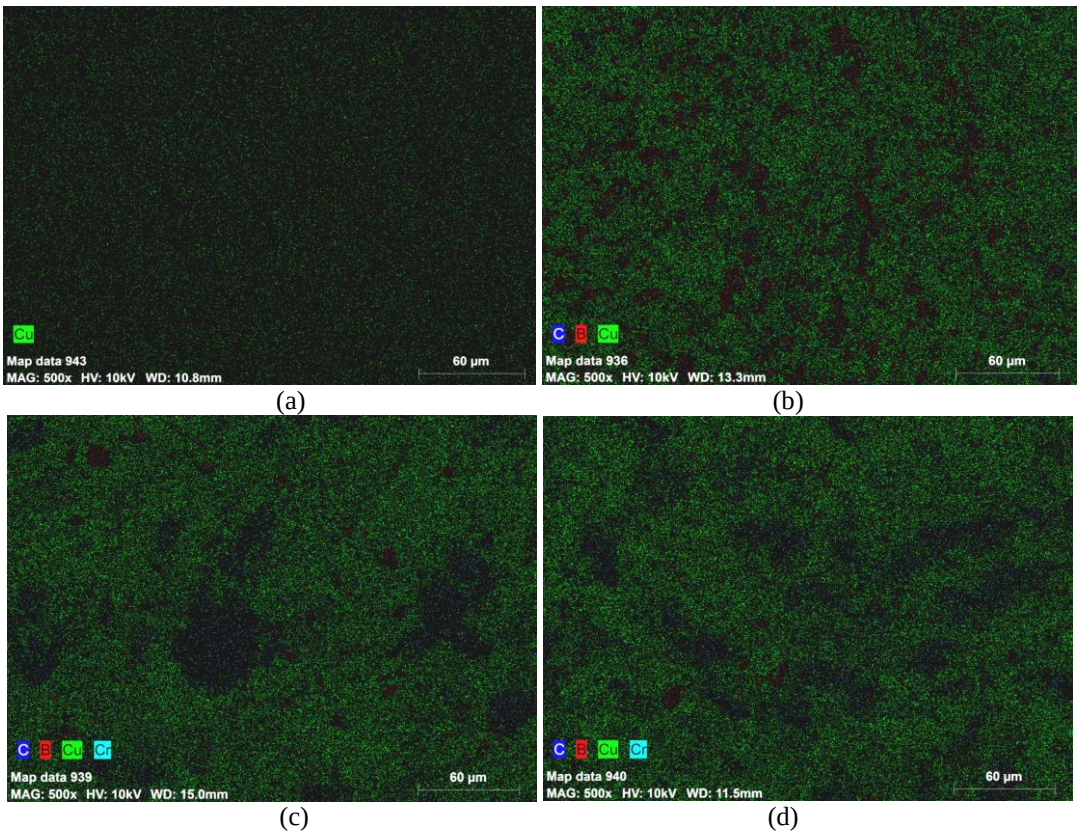

Figure 5. MAP-EDS analysis of: (a) Pure Cu, (b) Cu-8B_4C, (c) Cu-8B_4C-6Cr, and (d) Cu-8B_4C-6Cr-1CNF

Figure 6 shows the EDS analysis of Cu-8B_4C-6Cr-1CNF sample. Area 1 represents the Cu matrix. Small amounts of B, C and Cr also existed. Area 2 represents the B_4C grain. Small amounts of Cr and Cu contaminate particles of B_4C. Area 3 represents Cr in general, while small amounts of B, C, and Cu were identified in EDS analysis. The coexistence of B, C, Cr, and Cu in all three EDS analysis areas might be caused by mechanical bonding during the mechanical alloying. According to the EDS results, no oxide formation was detected in the microstructure. This result may suggest that no oxidation took place during the sintering process. Jha et al. [20] argued in their study on the friction and wear behaviours of Cu–4 wt.% Ni–TiC composites that there was no oxidation during sintering.

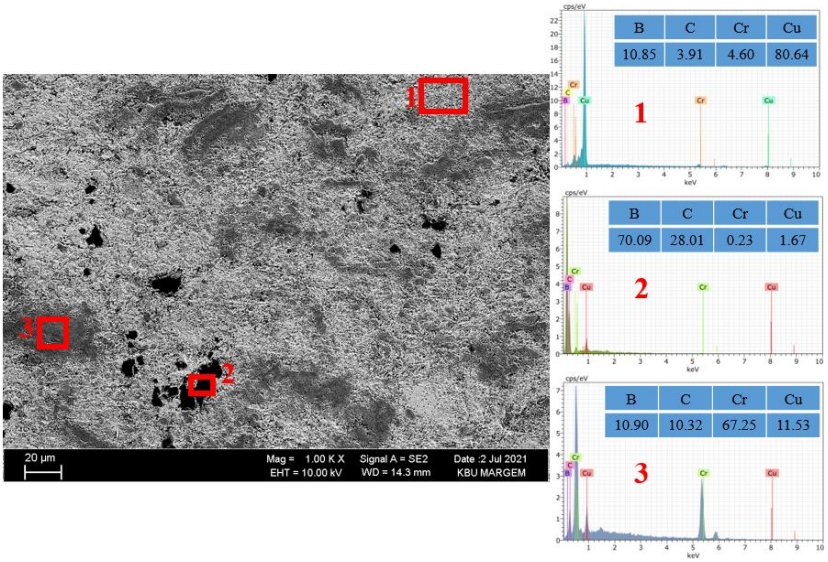

Figure 6. The EDS analysis of the Cu-8B_4C-6Cr-1CNF sample

Figure 7 shows the graphs generated following the XRD analysis performed to determine the phase of the samples. The pure Cu sample had the phase Cu (PDF card Cu 00-001-1241) with crystal planes (111), (200), (220), and (311). At 2-theta angles of 43.47°, 50.37°, 74.00°, and 89.93°, respectively, the Cu phase formed. CrB_2 (PDF card CrB_2 03-065-1883) and Cr_2B_3 (PDF card Cr_2B_3 00-37-1447) phases formed in addition to the Cu phase when the Cu matrix was reinforced with Cr, B_4C, and CNF. These phases had crystal planes (001) and (131), respectively. Also, the CrB_2 phase formed at a 2-theta angle of 29.10°, whereas the Cr_2B_3 phase formed at a 2-theta angle of 45.42°. In their study, Sun et al. [21] detected the Cr_2B_3 phase. Wang et al. [22] reported that they obtained the CrB_2 phase in their study on the sintering of B_4C and Cr_2O_3.

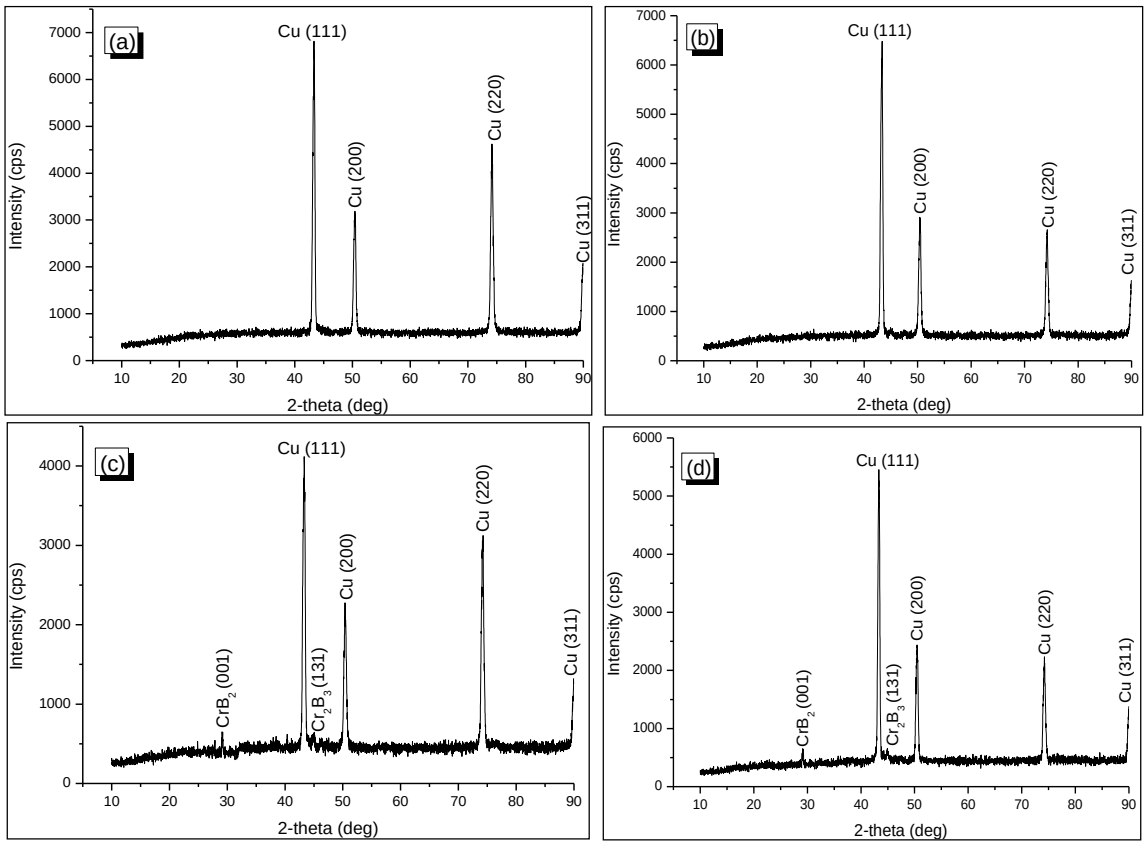

Figure 7. XRD graphs of samples of: (a) Pure Cu, (b) Cu-8B_4C, (c) Cu-8B_4C-6Cr, and (d) Cu-8B_4C-6Cr-1CNF

The graph in Figure 8 shows the experimental and relative densities of hybrid composites. In general, both the experimental and relative densities declined, depending on the increasing rate and type of reinforcing elements. The decline in experimental densities is due to the fact that the natural densities of chromium (7.19 g/cm^3), boron carbide (2.52 g/cm^3), and carbon nanofiber (1.9 g/cm^3) reinforcing elements are less than the density of copper (8.96 g/cm^3). The decline in relative densities stopped at Sample 3, peaked at Sample 6, and then resumed its decline. CNFs displayed the impact of filling the pores in Sample 6; on the other hand, in Samples 7 and 8, there was a decline in relative densities, partially due to aggregation of CNFs. The overall decline in relative densities can also be associated with the fact that the increased reinforcement rate had a negative impact on compressibility. Yet another reason is that the substantial difference in melting temperatures between the matrix and the reinforcing elements was a factor that prevented the particles' movements during sintering [23,24].

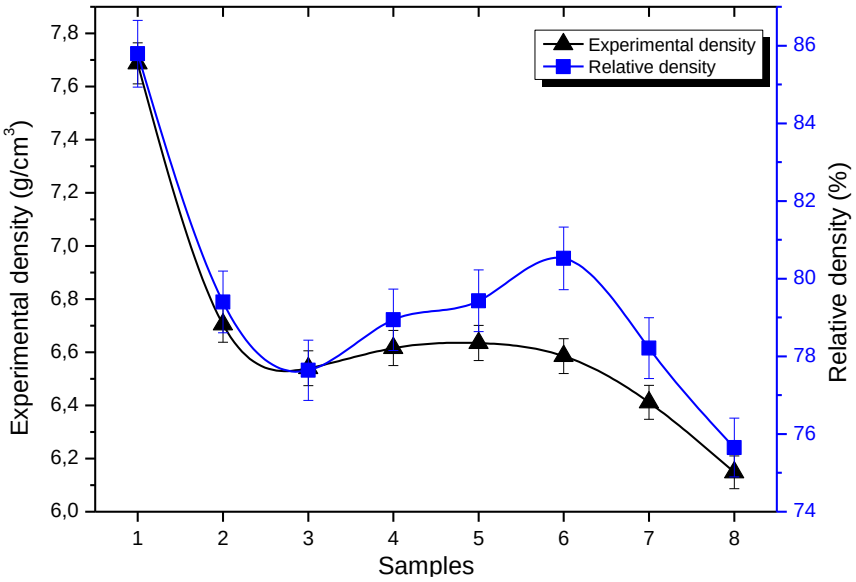

Figure 8. Experimental and relative densities of the samples

Figure 9 shows the hardness values of the samples. Hardness increased towards Sample 6 (maximum of 72.5 HB) among the Samples 1-6; on the other hand, the hardness of Samples 7 and 8 declined. The decline can be associated with the heterogeneous distribution of CNFs in Samples 7 and 8. In comparison to the pure Cu sample (Sample 1), there was an increase of approximately 54%. Here, B_4C, CNF, CrB_2, and Cr_2B_3 phases increased hardness by blocking movement of dislocations. In their study, Lim et al. reported that CNFs increased hardness by blocking movement of dislocations [25]. Islak et al. reported that the hardness of the samples produced by adding CNF to the bronze increased depending on the increasing amount of CNF [26].

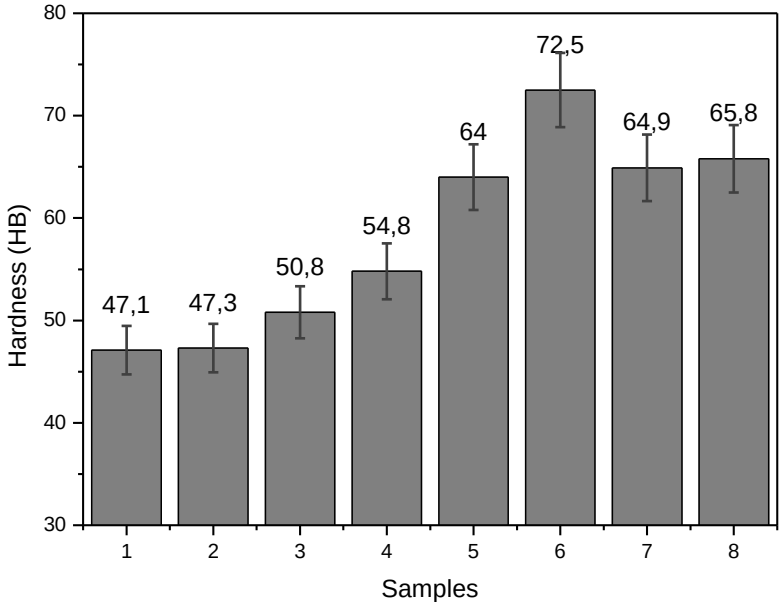

Figure 9. Hardness of the samples

4. Conclusions

The microstructure properties of Cu-Cr-B_4C-CNF hybrid composites produced by PM were thoroughly examined, and the following results were achieved:

1. PM was used to successfully produce Cu-Cr-B_4C-CNF hybrid composites. No cracks or discontinuities were noted in the samples.

2. Optical microscope images demonstrated that Cr and B_4C were partially homogeneously dispersed in the Cu matrix. CNFs could not be viewed with an optical microscope. Therefore, SEM images were captured at high magnifications, and clearly showed CNFs. Intermetallic phases, such as CrB_2 and Cr_2B_3, formed between the element B forming as a result of the degradation of B_4C and the Cr added to the matrix.

3. While the relative and experimental densities of the samples decreased with increasing reinforcement, there was an increase in hardness values up to Sample 6 and subsequently a partial decrease. Sample 6 had the maximum hardness observed in any sample (72.5 HB).

Competing Interest / Conflict of Interest

The authors declare that they have no competing interests.

Author Contribution

We declare that all Authors equally contribute.

5. References

[1] Islak, S., Çalıgülü, U., Hraam, H. R., Özorak, C., & Koç, V. (2019). Electrical conductivity, microstructure and wear properties of Cu-Mo coatings. Research on Engineering Structures and Materials, 5(2), 137-146.

[2] ASM Handbook: Properties and Selection: Nonferrous Alloys and Special-Purpose Materials, Vol.2, 10th ed., 1990.

[3] Deshpande, P. K., & Lin, R. Y. (2006). Wear resistance of WC particle reinforced copper matrix composites and the effect of porosity. Materials Science and Engineering: A, 418(1-2), 137-145.

[4] Buytoz, S., Dagdelen, F., Islak, S., Kok, M., Kir, D., & Ercan, E. (2014). Effect of the TiC content on microstructure and thermal properties of Cu–TiC composites prepared by powder metallurgy. Journal of Thermal Analysis and Calorimetry, 117(3), 1277-1283.

[5] Chen, H., Jia, C. C., & Li, S. J. (2013). Effect of sintering parameters on the microstructure and thermal conductivity of diamond/Cu composites prepared by high pressure and high temperature infiltration. International Journal of Minerals, Metallurgy, and Materials, 20(2), 180-186.

[6] Azimi, M., & Akbari, G. H. (2011). Development of nano-structure Cu–Zr alloys by the mechanical alloying process. Journal of Alloys and Compounds, 509(1), 27-32.

[7] Islamgaliev, R. K., Nesterov, K. M., Bourgon, J., Champion, Y., & Valiev, R. Z. (2014). Nanostructured Cu-Cr alloy with high strength and electrical conductivity. Journal of Applied Physics, 115(19), 194301.

[8] Correia, J. B., Davies, H. A., & Sellars, C. M. (1997). Strengthening in rapidly solidified age hardened Cu-Cr and Cu-Cr-Zr alloys. Acta Materialia, 45(1), 177-190.

[9] Islak, S., Kır, D., & Buytoz, S. (2014). Effect of sintering temperature on electrical and microstructure properties of hot pressed Cu-TiC composites. Science of Sintering, 46(1), 15-21.

[10] Rajkovic, V., Bozic, D., & Jovanovic, M. T. (2010). Effects of copper and Al_2O_3 particles on characteristics of Cu–Al_2O_3 composites. Materials & Design, 31(4), 1962-1970.

[11] Yin, J., Yao, D., Xia, Y., Zuo, K., & Zeng, Y. (2014). The effect of modified interfaces on the mechanical property of β-silicon nitride whiskers reinforced Cu matrix composites. Journal of alloys and compounds, 615, 983-988.

[12] Sule, R., Olubambi, P. A., Sigalas, I., Asante, J. K. O., & Garrett, J. C. (2014). Effect of SPS consolidation parameters on submicron Cu and Cu–CNT composites for thermal management. Powder Technology, 258, 198-205.

[13] Peng, W., & Sun, K. (2020). Effects of Cu/graphene interface on the mechanical properties of multilayer Cu/graphene composites. Mechanics of Materials, 141, 103270.

[14] Schubert, T., Zieliński, W., Michalski, A., Weißgärber, T., & Kieback, B. (2008). Interfacial characterization of Cu/diamond composites prepared by powder metallurgy for heat sink applications. Scripta Materialia, 58(4), 263-266.

[15] Torralba, J. D., Da Costa, C. E., & Velasco, F. (2003). P/M aluminum matrix composites: an overview. Journal of Materials Processing Technology, 133(1-2), 203-206.

[16] ASTM B962-17, Standard test methods for density of compacted or sintered powder metallurgy (PM) products using Archimedes' principle, ASTM International, 2017.
[17] TS EN ISO 6506-1:2014. "Metallic materials - Brinell hardness test - Part 1: Test method", TSE, Ankara, Türkiye.
[18] Akkaş, M., Islak, S., & Özorak, C. (2018). Corrosion and wear properties of Cu-TiC composites produced by hot pressing technique. Celal Bayar University Journal of Science, 14(4), 465-469.
[19] Lee, D. W., Ha, G. H., & Kim, B. K. (2001). Synthesis of Cu-Al_2O_3 nano composite powder. Scripta materialia, 44(8-9), 2137-2140.
[20] Jha, P., Gautam, R. K., & Tyagi, R. (2017). Friction and wear behavior of Cu–4 wt.% Ni–TiC composites under dry sliding conditions. Friction, 5(4), 437-446.
[21] Sun, Y. Z., Li, J. B., Wellburn, D., & Liu, C. S. (2016). Fabrication of wear-resistant layers with lamellar eutectic structure by laser surface alloying using the in situ reaction between Cr and B_4C. International Journal of Minerals, Metallurgy, and Materials, 23(11), 1294-1301.
[22] Wang, S., Xing, P., Gao, S., Yang, W., Zhuang, Y., & Feng, Z. (2018). Effect of in-situ formed CrB_2 on pressureless sintering of B4C. Ceramics International, 44(16), 20367-20374.
[23] Rahimian, M., Ehsani, N., Parvin, N., & reza Baharvandi, H. (2009). The effect of particle size, sintering temperature and sintering time on the properties of Al–Al_2O_3 composites, made by powder metallurgy. Journal of Materials Processing Technology, 209(14), 5387-5393.
[24] Islak, S., & Çelik, H. (2015). Effect of sintering temperature and boron carbide content on the wear behavior of hot pressed diamond cutting segments. Science of Sintering, 47(2), 131-143.
[25] Lim, J. Y., Oh, S. I., Kim, Y. C., Jee, K. K., Sung, Y. M., & Han, J. H. (2012). Effects of CNF dispersion on mechanical properties of CNF reinforced A7xxx nanocomposites. Materials Science and Engineering: A, 556, 337-342.
[26] Islak, S., Özorak, C., Abouacha, N. M. E., Çalıgülü, U., Koç, V., & Küçük, Ö. (2021). The effects of the CNF ratio on the microstructure, corrosion, and mechanical properties of CNF-reinforced diamond cutting tool. Diamond and Related Materials, 119, 108585.